Applied Surface Science 559 (2021) 149883

Contents lists available at ScienceDirect

Applied Surface Science

journal homepage: www.elsevier.com/locate/apsusc

Full Length Article

Surface composition of mixed self-assembled monolayers on Au by infrared attenuated total reflection spectroscopy

Angelo Tricase [a], Davide Blasi [a,b], Alessandro Favia [c], Angela Stefanachi [d], Francesco Leonetti [d], Giuseppe Colafemmina [a,b], Luisa Torsi [a,b,e], Gaetano Scamarcio [c,f,*]

[a] Dipartimento di Chimica, Università degli Studi di Bari "Aldo Moro", 70125 Bari, Italy
[b] Consorzio per lo Sviluppo dei Sistemi a Grande Interfase, 70125 Bari, Italy
[c] Dipartimento Interateneo di Fisica "M. Merlin", Università degli Studi di Bari "Aldo Moro", 70125 Bari, Italy
[d] Dipartimento di Farmacia - scienze del farmaco, Università degli Studi di Bari "Aldo Moro", 70125 Bari, Italy
[e] Faculty of Science and Engineering, Åbo Akademi University, 20500 Turku, Finland
[f] CNR, Istituto di Fotonica e Nanotecnologie, Sede di Bari, 70125 Bari, Italy

ARTICLE INFO

Keywords:
Self-assembled monolayers
Attenuated total reflection spectroscopy
Biofunctionalized interfaces

ABSTRACT

Self-assembled monolayers (SAMs) of *N*-(2-hydroxyethyl)-3-mercaptopropanamide (NMPA) were synthesized directly on the surface of electron-beam evaporated Au films, starting from 3-mercaptopropionic acid (3MPA) *via* ethyl-3-(3-dimethylamino-propyl)carbodiimide/N-hydroxysulfosuccinimide sodium salt (EDC/NHSS) coupling with ethanolamine hydrochloride. The influence on the reaction yield of the acidity of EDC/NHSS solutions (pH = 5.6 or 4.8) was assessed by exploiting the high surface sensitivity of infrared attenuated total reflection spectroscopy. The light-matter interaction was modeled in the framework of a matrix formalism considering the complete multi-layer sample structure. A comparison between the relative intensity of the main absorption bands, associated with *amide I* and carbonyl stretching of carboxylic acid or *amide II* vibrations, with a calibration curve obtained from the measurement of mixed 3MPA/NMPA SAMs, show that the more acid solution is 16% more efficient. This is mostly due to the higher protonation of the 3MPA.

1. Introduction

The recent development of ultra-sensitive biosensors based on biofunctionalized gold (Au) interfaces such as nanoparticle-mediated surface plasmon resonance (SPR) [1,2] or electrolyte-gated organic field effect transistors (EGOFETs) [3,4,5] has promoted a renewed interest on the molecular and supramolecular design of self-assembled monolayers (SAMs) [6,7,8,9]. These devices rely on thiol chemistry for the growth of biofunctionalized SAMs on the transduction Au surface. Such systems comprise *ad hoc* designed functionalities for anchoring the SAM of biorecognition elements. The functional groups include those that limit the non-specific interactions between the surface and the matrix [10,11,12], or reduce the Debye's screening, as in the case of EGOFET biosensors, [13,14]. This is very important for bioelectronic sensors design and fine-tuning of their performance figures of merit.

The compositional analysis of a SAM synthesized directly onto a surface is still a challenging task that needs to be addressed given the interest of these systems for many applications including biosensing [15,16,17]. The accurate analysis of the SAM composition and its impact on the supramolecular order are critical in the case of mixed SAMs synthesized directly at the metal surface. The related chemical reactions are influenced by many parameters, including pH, temperature, reactant concentration, solvent, and time, that can alter the foreseen reaction pathway leading to uncontrolled interphases [7,16,18]. Also, the steric constraints imposed from the high molecular packing, as in the case of SAMs, can inhibit the substrate reactivity leaving unreacted functional groups [19,20]. This is the case for SAMs containing terminal carboxylic functionalities, which are widely used in biosensors to anchor amine-containing bioreceptors *via* coupling to ethyl-3-(3-dimethylamino-propyl)carbodiimide/N-hydroxysulfosuccinimide sodium salt (EDC/NHSS) [21]. Through this powerful reaction, it is possible to convert the carboxylic groups into secondary amides directly in an aqueous medium, binding the bioreceptors to the SAM [22,23].

Since using the above synthetic strategy it is possible to covalently bind a huge amount of biomarkers that can reach a density of 10^{11}–10^{12} cm^{-2} [6,24], the assessment of the effective reaction yield (Y) related

* Corresponding author.
E-mail addresses: davide.blasi@uniba.it (D. Blasi), gaetano.scamarcio@uniba.it (G. Scamarcio).

https://doi.org/10.1016/j.apsusc.2021.149883
Received 9 January 2021; Received in revised form 31 March 2021; Accepted 19 April 2021
Available online 24 April 2021

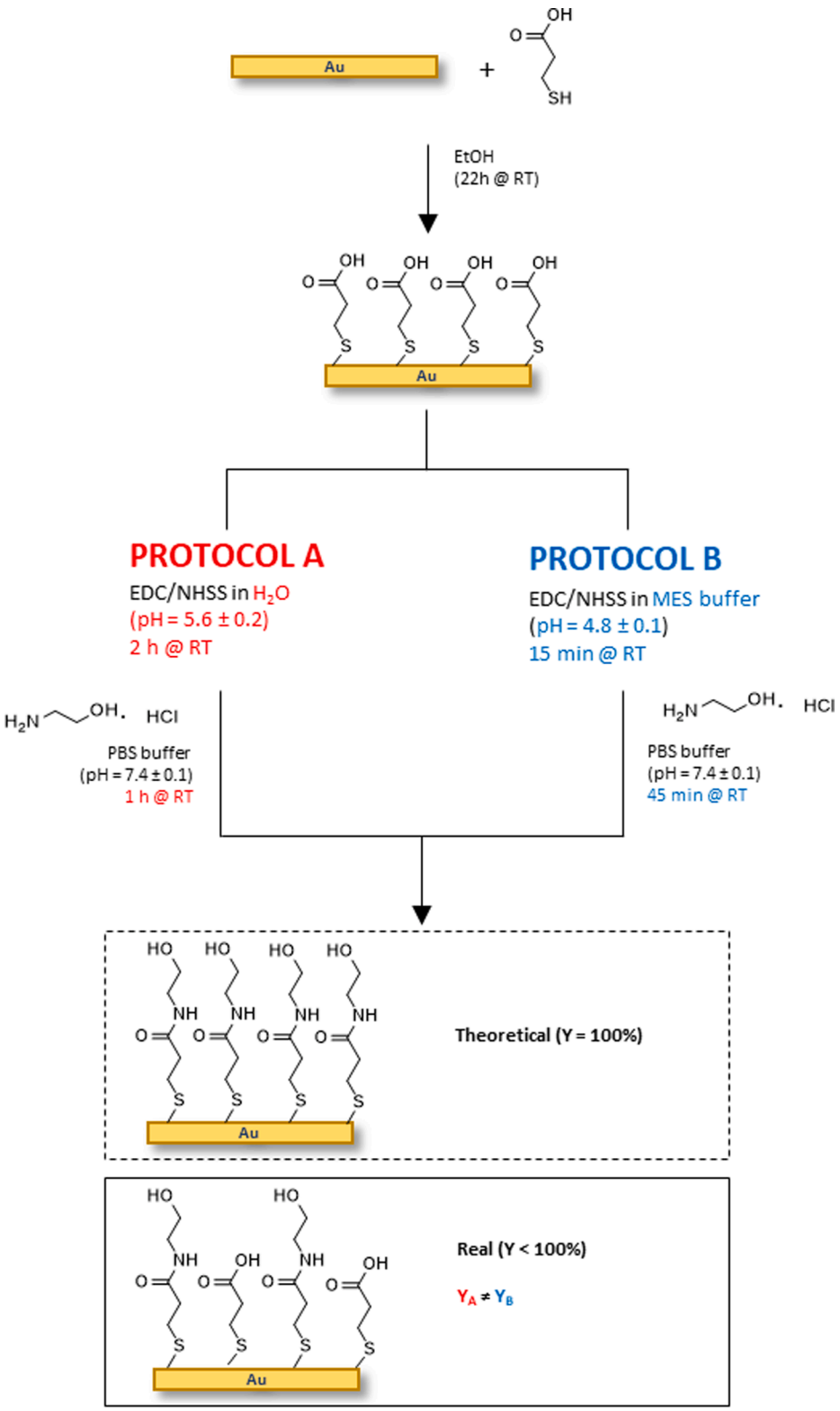

Fig. 1. Schematic representation of the functionalization reactions of gold surfaces. A SAM of 3MPA is grown on the gold surface. Carboxylic functionalities are activated by the EDC/NHSS mixture in different conditions addressed as protocol A and protocol B. Activated SAMs react with a solution of ethanolamine hydrochloride at different exposition times: for protocol A the time is 1 h while for protocol B the time is 45 min. The foreseen product, assuming a reaction yield of Y = 100%, is in both cases a SAM of NMPA.

with the conversion of carboxylic functionalities in amide groups is usually underestimated [16,17]. Nonetheless, the presence of unreacted carboxylic groups can strongly influence the interphase reactivity due to their pH sensitivity, generating electrostatic interactions that can promote or inhibit biorecognition events, determining changes in the surface wettability and, in the case of EGOFETs, affecting the formation of the electrical charge double layer [25,26].

This work aims at assessing the efficiency of the EDC/NHSS coupling comparing two different protocols for the synthesis of a *N*-(2-hydroxyethyl)-3-mercaptopropanamide (NMPA) SAM starting from a 3-mercaptopropionic acid (3MPA) SAM on electron-beam evaporated Au films (See Fig. 1) [24,27]. A main motivation for the present work arises from the evidence that EGOFET-based biosensors including a NMPA grafting layer leads to ultra-sensitive responses [24,28,29]. Accordingly,

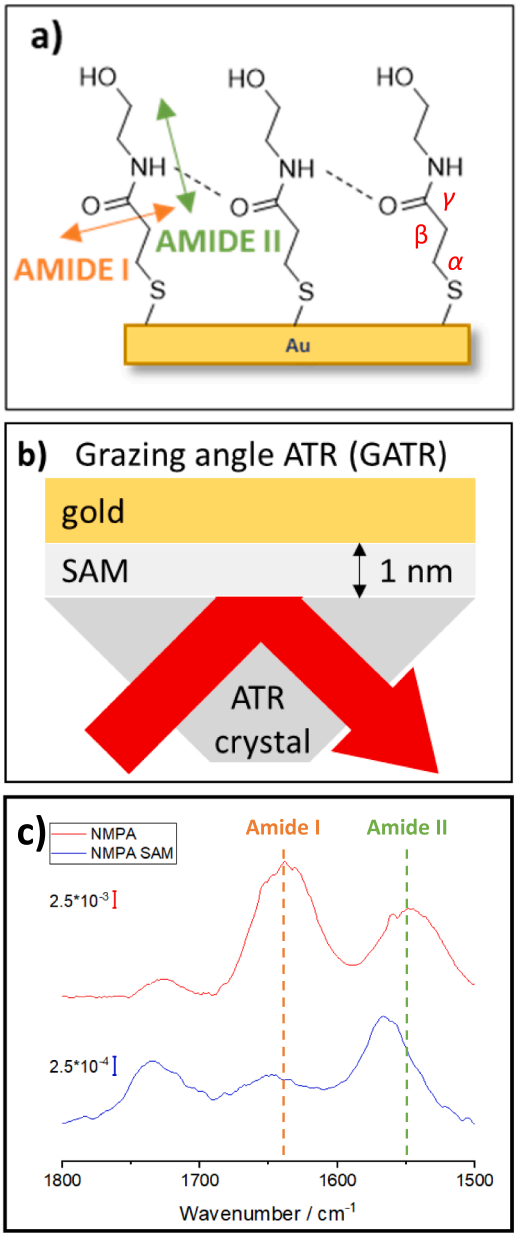

Fig. 2. a) Schematic structure of NMPA SAM on gold. The H-bonds (dash black lines) create a supramolecular configuration that determine the orientation of the NMPA chains and the dipole moments associated to the amide I and amide II vibrations. b) Scheme of infrared grazing angle attenuated total reflection (GATR). c) ATR absorbance spectrum of NMPA (red curve) and GATR spectrum of a NMPA SAM on a 50 nm-thick e-beam evaporated Au film deposited on a glass substrate (blue curve).

the study of analytical techniques able to assess the reaction yield of the synthesis of complex SAMs synthesized directly at the electrode surface is mandatory for the realization of reliable sensing platforms". Some preliminary studies on the composition of 3MPA SAMs before and after the EDC/NCSS activation were already performed using X-ray photoelectron spectroscopy [30] To this end, a spectroscopic investigation based on infrared (IR) attenuated total reflection (ATR) spectroscopy, was undertaken. While *in-situ* IR surface enhanced spectroscopic techniques have been recently demonstrated [17] the employed ATR approach is relatively simple and does not require any treatment of the Au substrate. Besides the relevance for the design of biosensing detecting interfaces, it is worth noting that this paper focuses on amide-containing SAMs having short aliphatic moiety and terminal hydroxyl groups that are expected to be endowed with good wettability properties and high degree of order.

A well-oriented and ordered network of NMPA SAM ideally forms the structure shown in Fig. 2**a**. SAMs containing secondary amides in the β and γ positions with respect to the sulphur atom, are stabilized by the formation of H-bonds among the protons of secondary amides and the carbonyl groups of neighbouring molecules [31,32,33,34,35,36]. Although the interactions between amide groups should dominate on the aliphatic ones, leading to the formation of an ordered H-bond network [34] in all the amide-containing SAMs studied up to now, the hydrophobic interactions are not negligible. Hence it was interesting to evaluate the supramolecular order of a NMPA SAM where the hydrophobic interactions are suppressed and a polar terminal group is present. We expected that due to the presence of an amide group in its γ position, the IR spectrum of a NMPA SAM should show the typical features of an ordered SAM. A NMPA SAM dominated by H-bond interactions is depicted in Fig. 2a.

In this configuration, the dipole moments of the amide groups have a well-defined orientation: the dipole associated with the carbonyl stretching of the amide I is almost parallel to the gold surface, whereas that associated with the N-H bending of the amide II lies almost perpendicular to the metal [32,36]. Interestingly, according to the so-called metal-surface selection rule, only the electric field component parallel to the plane of incidence of electromagnetic radiation (p-component) may interact with the sample surface [37,38]. Accordingly, in the IR spectra of an ordered NMPA SAM, the amide II signal is enhanced while the amide I one is suppressed with respect to a disordered system. IR spectroscopy of ultra-thin films grown on metallic substrates is particularly sensitive to these supramolecular configurations [37,38]. In fact, both the energy and the intensity ratio of amide I (1640 cm-1) and amide II (1550 cm-1) bands provide information on the orientation of alkyl chains in the SAM and the formation of H-bonds [32,36,39]. By comparing the ratio between the amide I and amide II ATR IR absorption bands with a calibration curve obtained studying mixed SAMs having controlled 3MPA and NMPA fractions, we have estimated the effective yield of the two functionalization protocols. The sample used for describing a pure NMPA SAM (Y = 100%) was prepared using the NMPA molecule synthesized using a procedure reported in literature [27].

2. Experimental

2.1. Sample preparation

3-Mercaptopronic Acid (98%), *N*-hydroxysulfosuccinimide sodium salt (NHSS), 1-ethyl-3-(3-dimethylamino-propyl)carbodiimide (EDC), and ethanolamine hydrochloride (EA) were purchased from Sigma-Aldrich and used without further purification. A 0.1 M 2-(*N*-morpholino)ethane-sulfonic acid (MES) buffer (Sigma-Aldrich) solution was adjusted with sodium hydroxide solution (NaOH 1 M) at pH 4.8 – 4.9. A phosphate buffered saline (PBS, Sigma-Aldrich) (phosphate buffer of 0.01 M, KCl of 0.0027 M, NaCl of 0.137 M) tablet was dissolved in 200 mL of HPLC water and used upon filtration on a Corning 0.22 μm polyethersulfone membrane. NMPA was synthesized starting from commercial 3MPA, and details on its synthesis are provided in a previous work [27].

Au surfaces were prepared on glass slides, by e-beam evaporation of a 5 nm-thick Ti adhesion layer followed by 50 nm-thick Au films. Prior to SAM deposition, the Au coated substrates were cleaned in boiling basic piranha solution (5:1:1 HPLC Water/NH_4OH 30%/H_2O_2 30%) for 10 min, rinsed with HPLC water, dried under N_2 flux and finally exposed to an ozone plasma for 10 min. SAMs were formed by soaking the Au coated substrates overnight in a 10 mM ethanol solution of 3MPA or NMPA at room temperature under N_2 atmosphere. 3MPA SAMs were treated by two different procedures, called *Protocol A* and *Protocol B*, and derived by precedent works of the research group (see Fig. 1) [4,27,30].

Both protocols comprise two steps, the exposition to an EDC/NHSS solution (0.2 M/0.05 M) to activate the carboxylic terminal groups and the immersion in a 1 M EA solution in PBS (pH = 7.4) to form secondary amides. In protocol A the EDC/NHSS solution was prepared in HPLC water (pH = 5.6), the activation step was carried out for 2 h, and the EA exposition for 1 h. In protocol B the EDC/NHSS solution was prepared in MES buffer solution (pH = 4.8), the activation steps were carried out for 15 min and the EA exposition for 45 min. The samples with a controlled amount of NMPA used for the determination of the calibration curve were prepared immersing the substrate on the thiol solution with a controlled molar ratio of 3MPA and NMPA especially the followed molar ratio were used: 3MPA:NMPA = 1:5, 3MPA:NMPA = 2:3, 3MPA:NMPA = 1:1, and 3MPA:NMPA = 3:2.

2.2. Infrared attenuated total reflection spectroscopy

IR spectra were measured by using a Perkin Elmer Spectrum Two FT-IR spectrometer equipped with an ATR module including a diamond crystal at a fixed 45° incidence angle. The air gap between the sample and the diamond crystal was minimized and assumed negligible by progressively increasing the applied pressure using a dedicated mechanical tool while checking for signal saturation. Each spectrum was mediated over 64 scans in the range 400–4000 cm^{-1}, at a spectral resolution of 2 cm^{-1}. Spectral smoothing is carried out using a 21-points sliding average data window approach. The experimental configuration schematically shown in Fig. 2**b** is very similar to experimental schemes named grazing angle ATR (GATR) [40,41], or metal-underlayer ATR [42]. Particularly, the presence of the SAM/metal interface in close proximity with the ATR crystal/SAM interface strongly enhances the conventional ATR signal up to ~ 2 orders of magnitude [43,44] and allows to measure the infrared absorbance spectrum even of an ultra-thin (<1 nm-thick) film. [45] In fact, it has been shown that the ATR spectra of alkylthiol based SAMs grown on Au or Pd metals, recorded using a Ge ATR crystal and an incident angle of 65° are identical to the absorbance spectra obtained by polarization modulation-infrared reflection-adsorption spectroscopy (PM-IRRAS) under truly grazing incidence (83°) [41]. On the other hand, it is worth noting that in the case of SAMs deposited on metallic films, a high reflectivity and large ATR signals are expected also using ATR crystals different form Ge at lower incidence angle. In fact, using the model described in the next paragraph to calculate the ATR spectrum of a SAM deposited on a Au film, put in intimate contact with an diamond ATR crystal under an incidence angle of 45°, we estimated an enhancement factor of 2 with respect to the case of a SAM deposited directly on diamond. Accordingly, in this report the ATR spectra measured on SAMs grown on Au are addressed as GATR.

2.3. Modelling GATR spectra

The light-matter interaction with a multi-layer structure, as schematically shown in Fig. 2**b**, was calculated employing a matrix formalism [46]. For each *j*-th layer, a two-dimensional optical (electric field) amplitude vector is defined, with components $A_j^+(z)$ and $A_j^-(z)$, corresponding to light propagation in the positive and negative directions along the z-axis normal to the interfaces. The phase Φ_j picked up during propagation between points $z = 0$and $z = d_j$ in a medium of refractive index $n_j(k)$ and thickness d_j depends on the complex dielectric function of the medium. Considering light propagating with incidence angle θ from a medium of complex refractive index $n_0(k)$, then $\Phi_j = 2\pi k d_j \sqrt{n_j^2 - n_0^2 \sin^2\theta}$.

The amplitudes at points $z = 0$and $z = d_j$ of the *j*-th layer, are linked through the general form of the propagation matrix $\mathscr{P}_j$, as:

$$\begin{pmatrix} A_j^+(d_j) \\ A_j^-(d_j) \end{pmatrix} = \begin{pmatrix} e^{i\Phi_j} & 0 \\ 0 & e^{-i\Phi_j} \end{pmatrix} \begin{pmatrix} A_j^+(0) \\ A_j^-(0) \end{pmatrix}$$

The amplitudes at points $z = d_{j-1}$ of the *(j-1)*-th layer and $z = 0$ of the *j*-th layer, are linked through the interface matrix $\mathscr{I}_{j-1,j}$, containing the polarization dependent Fresnel coefficients $r_{a,b}$ for reflectivity and $t_{a,b}$ for transmittivity at the *a*-*b* interface as:

$$\begin{pmatrix} A_j^+(0) \\ A_j^-(0) \end{pmatrix} = \frac{1}{t_{j,j-1}} \begin{pmatrix} 1 & r_{j,j-1} \\ -r_{j-1,j} & 1 \end{pmatrix} \begin{pmatrix} A_{j-1}^+(d_{j-1}) \\ A_{j-1}^-(d_{j-1}) \end{pmatrix}$$

The matrix $\mathscr{M}$ describing the whole multi-layered system, i.e. linking the incident amplitude A_{in} with the reflected A_r and transmitted A_t ones, is then computed by matrix multiplication over all *N* layers:

$$\begin{pmatrix} A_t \\ 0 \end{pmatrix} = \left(\prod_{j=2}^{N} \mathscr{I}_{j,j+1} \mathscr{P}_j \right) \mathscr{I}_{1,2} \begin{pmatrix} A_{in} \\ A_n \end{pmatrix} \equiv \mathscr{M} \begin{pmatrix} A_{in} \\ A_n \end{pmatrix}$$

The reflectance amplitude is then extracted as $\rho = -\mathscr{M}_{21}/\mathscr{M}_{22}$.

In applying this model to the sample under examination, the optical constants are taken from the literature [47] for all media but the SAM. The SAM refractive index was modeled considering the contribution of a set of $b = 3$ harmonic oscillators to the polarizability α and the Clausius-Mossotti equation. The number of harmonic oscillators was chosen upon inspection of the experimental spectra, which confirmed the presence of two peaks in the amide I and amide II positions as well as a third band due to possible contamination. Each j-th harmonic oscillator results in a resonance associated with Lorentzian parameters F_j, k_j and Γ_j. F_j is the oscillator strength, which quantifies the response to the applied field; k_j is the resonance wavenumber, related to the center of the peak; Γ_j is the full width at half maximum (FWHM) of the peak. Properly defining also the density of molecules N and the electronic polarizability α_0 – i.e. the medium polarizability far from resonances, – the expressions for the polarizability and the refractive index read:

$$\alpha(k) = \alpha_0 + c_0 \sum_{j=1}^{b} \frac{F_j}{k_j^2 - k^2 + i\Gamma_j k}; \quad [n(k)]^2 = \varepsilon(k) = 1 + \frac{4\pi N\alpha(k)}{1 - \frac{4\pi}{3} N\alpha(k)}.$$

The factor $N{\cdot}c_0 = 1.2{\cdot}10^5$ cm^{-2} comprises constant contributions deriving from first principle evaluation of α in the Lorentz model [46]. F_j are left as fitting parameters by means of chi square minimization. The value of α_0 is set so that of SAM refractive index far from any resonance is 1.45, a value widely agreed upon for similar SAMs [48].

3. Results and discussion

3.1. GATR spectra of NMPA and 3MPA SAMs

The upmost curve in Fig. 2c shows the ATR spectrum in the infrared range of the amide vibrations, of a thick bulk-like NMPA film deposited directly on the ATR diamond crystal by dropping pure NMPA, which is a viscous liquid. The two bands at 1640 ± 1 cm^{-1} and 1545 ± 1 cm^{-1} are due to amide I and amide II vibrations, respectively. Note that in the above energy range, the infrared evanescent wave probes the bulk sample within a length of ~ 1 μm, and the relative intensity of the two bands corresponds to a random orientation of the NMPA chains in the liquid phase.

The bottommost curve in Fig. 2**c** shows the GATR spectrum of a NMPA SAM grown on Au. Both the amide II (1565 ± 1 cm^{-1}) and amide I (1650 ± 1 cm^{-1}) bands are blue-shifted with respect to the bulk sample, due to the formation of an H-bond network among SAM molecules. As expected from the metal-surface selection rule, the intensity ratio between amide I and amide II bands (0.56) is almost inverted with respect to the bulk value (1.48) where the molecules are randomly oriented. The band at 1740 ± 1 cm^{-1} is ascribed to traces of fatty acids

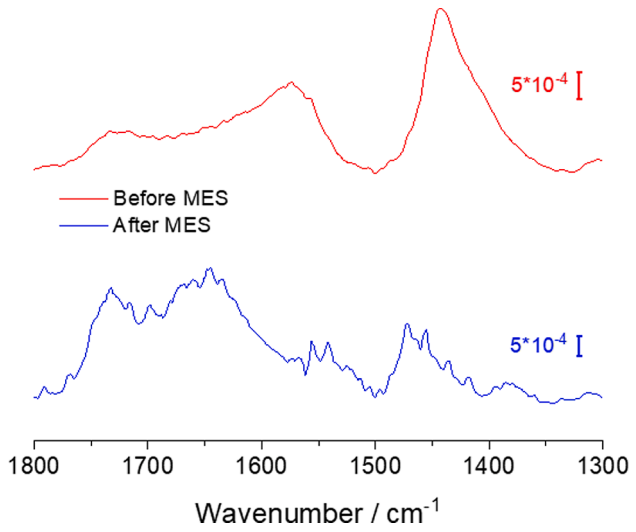

Fig. 3. GATR spectra of a 3MPA SAM on Au from an ethanol solution (red curve) and after the exposition to a MES buffered solution at pH = 4.8 (blue curve).

on the substrate since it is observed also on bare gold after the cleaning procedure (data not shown) and in all the other samples. However, the blue shift of the amide I and amide II bands confirms that the formation of an extended H-Bond structure in the SAM structure [32] confirming a limited effect of this contaminant in NMPA SAM growth. The relative high intensity of this band is ascribed to a longer chain length of the hypothesized contaminant, compatible with the contamination of a very high absorbance molecule on a limited sample area [49].

These results are in excellent agreement with previous reports [34], support the notion of the formation of a highly ordered configuration of the γ-amide SAM even without presenting an extended aliphatic moiety, and confirms the main role of the amide group in ordering the molecules on the gold surface. The bottommost spectrum of Fig. 2c is given by a SAM prepared using directly the NMPA thiol previously synthesized. Ideally, this spectrum represents the limit case in which a NMPA SAM is synthesized starting from a 3MPA SAM with a reaction yield (Y) of 100% (all the 3MPA molecules are converted in NMPA ones. The other limit case (Y = 0%) is given by a 3MPA SAM, that is our starting point system (see Fig. 3).

The upmost curve in Fig. 3 shows the GATR spectrum of a 3MPA SAM on Au. Interestingly, the analysis of the IR spectrum depicts a sample with a high degree of deprotonation of carboxylic groups."

The spectrum exhibits the signals of the symmetric (1572 ± 1 cm^{-1}) and asymmetric (1441 ± 1 cm^{-1}) deprotonated carboxylic acid stretching, whereas the protonated carboxylic acid C = O stretching (around 1650 cm^{-1}) results not visible. This finding points out the importance of the pH control in the EDC/NHSS coupling. In fact, a carboxylate SAM cannot react with the carbodiimide, resulting in a poor activation yield [17]. In order to protonate the 3MPA SAM, the sample was immersed in a MES buffered solution at pH = 4.8 for fifteen minutes (the same solution and the same time used in the activation step of the protocol B). The GATR spectrum of the acidified SAM is reported in the bottommost curve of Fig. 3: the new main peak at 1651 cm^{-1} is ascribed to the carbonyl stretching of carboxylic acid. From now on if not specified differently, we mention 3MPA SAM after MES.

3.2. GATR spectra of 3MPA:NMPA mixed SAMs – Calibration curve

The starting point to obtain a calibration curve for the determination of the reaction yield of the EDC/NHSS coupling is the measurement of the GATR spectra of NMPA and 3MPA SAMs, corresponding to Y = 100% and Y = 0%, respectively. Fig. 4**a and 4b** show representative GATR spectra of 3MPA after MES and NMPA SAMs, respectively. The solid lines in Fig. 4 are the best fit GATR spectra calculated following the procedure outlined in the paragraph 2.4. The statistical error is quantified in 3 10^{-5} absorbance units for both spectra and normalized chi square minimization resulted in 5.98 (3MPA SAM) and 1.06 (NMPA SAM), suggesting a good agreement. The ratio $R_Y = \frac{\int_{1610}^{1690} S(k)dk}{\int_{1500}^{1580} S(k)dk}$ between the spectral areas of the spectrum S in the wavenumber ranges Δk = 1610–1690 cm^{-1} (where the amide I and carbonyl stretching of carboxylic acid bands are dominant) and Δk = 1500–1580 cm^{-1} (where the amide II band is dominant) is a spectroscopic parameter linearly proportional to Y. We have found the values $R_{Y=0\%} = 3.12 \pm 0.38$ and $R_{Y=100\%} = 0.80 \pm 0.11$. Consequently, the actual NMPA content Y in the investigated mixed SAMs can be estimated from the measured R_Y value using the simple linear relationship $Y[\%] = 100\frac{R_{0\%}-R_Y}{R_{0\%}-R_{100\%}}$ [46].

To test the linear dependence, mixed SAMs of 3MPA:NMPA have been prepared and the corresponding R_Y ratios have been extracted from

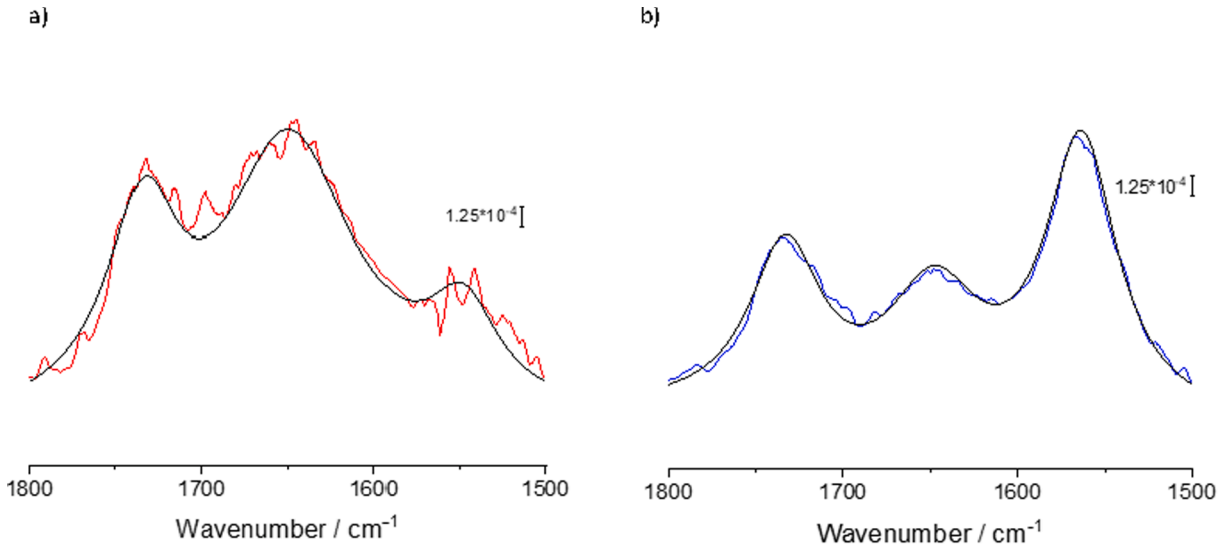

Fig. 4. (a) GATR spectrum of a 3MPA SAM after MES on Au(red curve). Same data of the bottommost panel of Fig. 3 in a limited spectral range. (b) GATR spectrum of NMPA SAM (blue curve) on Au. Same data of the bottommost panel in Fig. 2c in a limited spectral range. The black curves are best fit calculated as described in the paragraph 2.4.

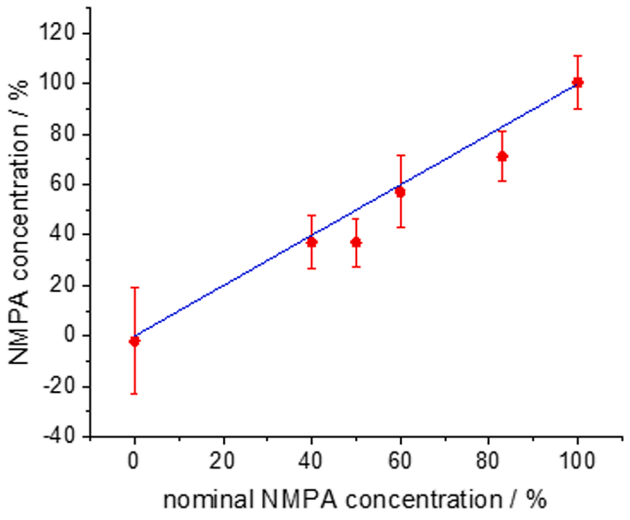

Fig. 5. NMPA concentration of mixed SAMs estimated by the analysis of GATR spectra as a function of the nominal concentrations. The solid line corresponds to the linear correlation.

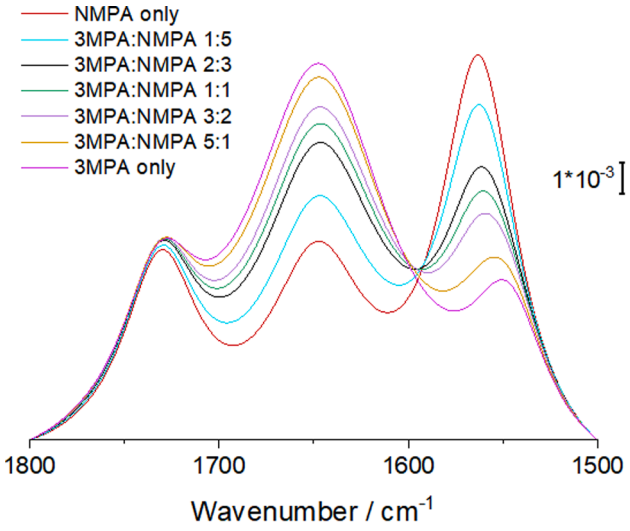

Fig. 6. Representative GATR spectra of 3MPA:NMPA mixed SAMs calculated as described in the paragraph 2.4 using the parameters used to fit the theory to the spectra of Fig. 4.

the analysis of the measured GATR spectra. The resulting nominal percentage values of NMPA are: 83% (3MPA:NMPA = 1:5), 60% (3MPA:NMPA = 2:3), 50% (3MPA:NMPA = 1:1), and 40% (3MPA:NMPA = 3:2). All samples were treated with the MES buffered solution to protonate all the carboxylic groups. Fig. 5 shows that a linear correlation exists between the percentage values of NMPA in the mixed SAMs as measured by GATR, and the nominal ones. The solid line in Fig. 5 shows the trend of Y, as extracted from the calculated GATR spectra (see Fig. 6). The theoretical and experimental data sets are compared by means of normalized chi square evaluation, which results in a value of 1.2 with three degrees of freedom. Comparison with statistical tables shows that the assumed hypothesis should be accepted.

3.3. Reaction yields extracted from the analysis of GATR spectra

Fig. 7 shows representative GATR spectra corresponding to NMPA SAMs synthesized *in situ* following the protocol A and protocol B. Six samples for each protocol were prepared and measured. For the SAMs prepared with the protocol A we found $R_Y = 1.81 \pm 0.16$ while for the

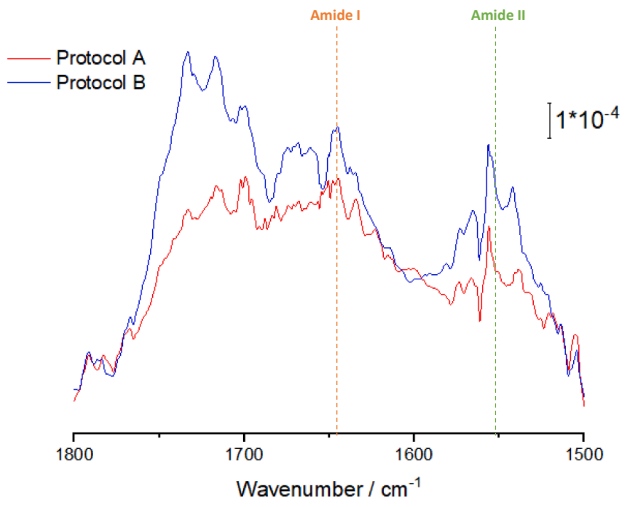

Fig. 7. Representative GATR spectra of NMPA SAMs synthesized *in situ* with the Protocol A (red curve) and Protocol B (blue curve).

protocol B we found $R_Y = 1.60 \pm 0.14$, corresponding to yields $Y_A = 56.4 \pm 7\%$ and $Y_B = 65.5 \pm 8\%$.

These values are substantially lower than the yield reported for the EDC/NHS coupling of carboxylic acid dispersed in solution, which is typically around 80% [50]. The decrease for in-surface reaction is probably due to the inter-chain steric hindrance [20] and the reaction between free and activated carboxylic acid [16,19]. Moreover, a yield lower than 20% is reported for more packed surface, such as Poly-Metacrylic Acid (PMAA) immobilized on SiO_2 surfaces [19], probably due to the promotion of anhydrides formation in highly packed systems. Our work suggests an intermediate scenario between the free carboxylic acid in solution [50] and the PMAA on surface [19]. Our scenario can be compared to the semi-quantitative analysis on carboxylic acid SAMs, where the value Y = 60% was found working in excess of EDC, as in our protocols [16].

The slightly different yields between the two protocols may be related to the different pH values and the time of the activation step. The higher Y value in the case of protocol B can be explained considering that a more acidic and buffered pH should lead to a higher protonation of the 3MPA SAM that, after its deposition is almost completely in the carboxylate form [17]; a shorter time of activation should limit the 3MPA SAM deactivation due to the hydrolysis reaction the succinimidic ester formed between 3MPA and NHSS [19]. In fact, the GATR spectra of the two SAMs are quite different as can be seen in Fig. 7. In both cases it is possible to identify the target signals, but the intensity ratio for the two SAMs is different; in particular the SAM synthesized with the protocol A presents a higher amide I/amide II ratio.

4. Conclusions

Self-assembled monolayers grown on the surface of transducing elements play a central role for the development of biosensors such as electrolyte-gated organic field effect transistors. The assessment of the composition of SAMs synthesized directly onto a surface is still challenging. In this report we have shown that the analysis of infrared attenuated total reflection spectra, modelling the light-matter interaction in the framework of a matrix formalism considering the actual multi-layer structure is a non-invasive effective approach allowing to determine the reaction yield as a function of the pH of the solution. Significantly, the effectiveness of this approach was demonstrated for the first time in amide-containing SAMs having short aliphatic moiety and terminal hydroxyl groups.

CRediT authorship contribution statement

Angelo Tricase: Conceptualization, Investigation, Writing - original draft. **Davide Blasi:** Conceptualization, Investigation, Writing - original draft. **Alessandro Favia:** Formal analysis, Software, Investigation, Writing - original draft. **Angela Stefanachi:** Resources. **Francesco Leonetti:** Resources. **Giuseppe Colafemmina:** Resources. **Luisa Torsi:** Supervision, Funding acquisition. **Gaetano Scamarcio:** Supervision, Conceptualization, Methodology, Writing - review & editing.

Declaration of Competing Interest

The authors declare that they have no known competing financial interests or personal relationships that could have appeared to influence the work reported in this paper.

Acknowledgments

This work was partly supported by the European Union's Horizon 2020 research and innovation programme SiMBiT [grant agreement No. 824946]; the Italian ministry MIUR [grants e-DESIGN (ARS01_01158); PMGB (ARS01_01195); IDF SHARID (ARS01_01270)]; the Academy of Finland [projects #316881, #316883, #332106]; Åbo Akademi University and CSGI (Consorzio Interuniversitario per lo Sviluppo dei Sistemi a Grandi Interfasi)

References

[1] S. Zeng, D. Baillargeat, H.P. Ho, K.T. Yong, Nanomaterials enhanced surface plasmon resonance for biological and chemical sensing applications, Chem. Soc. Rev. 43 (2014) 3426–3452, https://doi.org/10.1039/c3cs60479a.
[2] F. Fathi, M.R. Rashidi, Y. Omidi, Ultra-sensitive detection by metal nanoparticles-mediated enhanced SPR biosensors, Talanta 192 (2019) 118–127, https://doi.org/10.1016/j.talanta.2018.09.023.
[3] R.A. Picca, K. Manoli, E. Macchia, L. Sarcina, C. Di Franco, N. Cioffi, D. Blasi, R. Österbacka, F. Torricelli, G. Scamarcio, L. Torsi, Ultimately sensitive organic bioelectronic transistor sensors by materials and device structure design, Adv. Funct. Mater. 30 (2020) 1904513, https://doi.org/10.1002/adfm.201904513.
[4] E. Macchia, R.A. Picca, K. Manoli, C. Di Franco, D. Blasi, L. Sarcina, N. Ditaranto, N. Cioffi, R. Österbacka, G. Scamarcio, F. Torricelli, L. Torsi, About the amplification factors in organic bioelectronic sensors, Mater. Horizons. 7 (2020) 999–1013, https://doi.org/10.1039/c9mh01544b.
[5] E. Macchia, K. Manoli, C. Di Franco, G. Scamarcio, L. Torsi, New trends in single-molecule bioanalytical detection, Anal. Bioanal. Chem. 412 (2020) 5005–5014, https://doi.org/10.1007/s00216-020-02540-9.
[6] L. Li, S. Wang, Y. Xiao, Y. Wang, Recent advances in immobilization strategies for biomolecules in sensors using organic field-effect transistors, Trans. Tianjin Univ. (2020), https://doi.org/10.1007/s12209-020-00234-y.
[7] A. Badia, R.B. Lennox, L. Reven, A dynamic view of self-assembled monolayers, Acc. Chem. Res. 33 (2000) 475–481, https://doi.org/10.1021/ar9702841.
[8] S. Casalini, C.A. Bortolotti, F. Leonardi, F. Biscarini, Self-assembled monolayers in organic electronics, Chem. Soc. Rev. 46 (2017) 40–71, https://doi.org/10.1039/c6cs00509h.
[9] F. Leonardi, A. Tamayo, S. Casalini, M. Mas-Torrent, Modification of the gate electrode by self-assembled monolayers in flexible electrolyte-gated organic field effect transistors: Work function, Vs. capacitance effects, RSC Adv. 8 (2018) 27509–27515, https://doi.org/10.1039/c8ra05300f.
[10] N. Patel, M.C. Davies, R.J. Heaton, C.J. Roberts, S.J.B. Tendler, P.M. Williams, A scanning probemicroscopy study of the physisorption and chemisorption of protein molecules onto carboxylate terminated self-assembledmonolayers, Appl. Phys. A Mater. Sci. Process. 66 (1998) 569–574, https://doi.org/10.1007/s003390051203.
[11] D. Ataman Sadık, H. Eksi-Kocak, G. Ertaş, İ.H. Boyacı, M. Mutlu, Mixed-monolayer of N-hydroxysuccinimide-terminated cross-linker and short alkanethiol to improve the efficiency of biomolecule binding for biosensing, Surf. Interface Anal. 50 (2018) 866–878, https://doi.org/10.1002/sia.6489.
[12] V. Parkula, M. Berto, C. Diacci, B. Patrahau, M. Di Lauro, A. Kovtun, A. Liscio, M. Sensi, P. Samorì, P. Greco, C.A. Bortolotti, F. Biscarini, Harnessing selectivity and sensitivity in electronic biosensing: a novel lab-on-chip multigate organic transistor, Anal. Chem. 92 (2020) 9330–9337, https://doi.org/10.1021/acs.analchem.0c01655.
[13] N. Haustein, Ó. Gutiérrez-Sanz, A. Tarasov, Analytical model to describe the effect of polyethylene glycol on ionic screening of analyte charges in transistor-based immunosensing, ACS Sensors 4 (2019) 874–882, https://doi.org/10.1021/acssensors.8b01515.
[14] M.Á. García-Chamé, Ó. Gutiérrez-Sanz, E. Ercan-Herbst, N. Haustein, M.S. Filipiak, D.E. Ehrnhöfer, A. Tarasov, A transistor-based label-free immunosensor for rapid detection of tau protein, Biosens. Bioelectron. 159 (2020) 1–6, https://doi.org/10.1016/j.bios.2020.112129.
[15] S. Boujday, M.L. de la Chapelle, J. Srajer, W. Knoll, Enhanced vibrational spectroscopies as tools for small molecule biosensing, Sensors (Switzerland). 15 (2015) 21239–21264, https://doi.org/10.3390/s150921239.
[16] S. Sam, L. Touahir, J. Salvador Andresa, P. Allongue, J.N. Chazalviel, A.C. Gouget-Laemmel, C.H. De Villeneuve, A. Moraillon, F. Ozanam, N. Gabouze, S. Djebbar, Semiquantitative study of the EDC/NHS activation of acid terminal groups at modified porous silicon surfaces, Langmuir 26 (2010) 809–814, https://doi.org/10.1021/la902220a.
[17] T.C. Tsai, C.W. Liu, Y.C. Wu, N.A.P. Ondevilla, M. Osawa, H.C. Chang, In situ study of EDC/NHS immobilization on gold surface based on attenuated total reflection surface-enhanced infrared absorption spectroscopy (ATR-SEIRAS), Colloids Surfaces B Biointerfaces. 175 (2019) 300–305, https://doi.org/10.1016/j.colsurfb.2018.12.009.
[18] F. Schreiber, Structure and growth of self-assembling monolayers, Prog. Surf. Sci. 65 (2000) 151–257, https://doi.org/10.1016/S0079-6816(00)00024-1.
[19] Q. Yan, H.N. Zheng, C. Jiang, K. Li, S.J. Xiao, EDC/NHS activation mechanism of polymethacrylic acid: Anhydride versus NHS-ester, RSC Adv. 5 (2015) 69939–69947, https://doi.org/10.1039/c5ra13844b.
[20] T. Sawaguchi, Y. Sato, F. Mizutani, In situ scanning tunneling microscopy observation of self-assembled monolayers of 3-mercaptopropionic acid on Au(111) in perchloric acid solution, J. Electroanal. Chem. 507 (2001) 256–262. https://doi.org/https://doi.org/10.1016/S0022-0728(01)00362-X.
[21] K.A. Totaro, X. Liao, K. Bhattacharya, J.I. Finneman, J.B. Sperry, M.A. Massa, J. Thorn, S.V. Ho, B.L. Pentelute, Systematic investigation of EDC/sNHS-mediated bioconjugation reactions for carboxylated peptide substrates, Bioconjug. Chem. 27 (2016) 994–1004, https://doi.org/10.1021/acs.bioconjchem.6b00043.
[22] J.W. Lee, S.J. Sim, S.M. Cho, J. Lee, Characterization of a self-assembled monolayer of thiol on a gold surface and the fabrication of a biosensor chip based on surface plasmon resonance for detecting anti-GAD antibody, Biosens. Bioelectron. 20 (2005) 1422–1427, https://doi.org/10.1016/j.bios.2004.04.017.
[23] N. Xia, Y. Xing, G. Wang, Q. Feng, Q. Chen, H. Feng, X. Sun, L. Liu, Probing of EDC/NHSS-mediated covalent coupling reaction by the immobilization of electrochemically active biomolecules, Int. J. Electrochem. Sci. 8 (2013) 2459–2467.
[24] E. Macchia, K. Manoli, B. Holzer, C. Di Franco, M. Ghittorelli, F. Torricelli, D. Alberga, G.F. Mangiatordi, G. Palazzo, G. Scamarcio, L. Torsi, Single-molecule detection with a millimetre-sized transistor, Nat. Commun. 9 (2018), https://doi.org/10.1038/s41467-018-05235-z.
[25] S. Chen, L. Liu, J. Zhou, S. Jiang, Controlling antibody orientation on charged self-assembled monolayers, Langmuir 19 (2003) 2859–2864, https://doi.org/10.1021/la026498v.
[26] J.C. Everts, M. Ravnik, Complex electric double layers in charged topological colloids, Sci. Rep. 8 (2018) 14119, https://doi.org/10.1038/s41598-018-32550-8.
[27] D. Blasi, L. Sarcina, A. Tricase, A. Stefanachi, F. Leonetti, D. Alberga, G. F. Mangiatordi, K. Manoli, G. Scamarcio, R.A. Picca, L. Torsi, Enhancing the sensitivity of biotinylated surfaces by tailoring the design of the mixed self-assembled monolayers synthesis, ACS Omega 5 (2020) 16762–16771, https://doi.org/10.1021/acsomega.0c01717.
[28] E. Macchia, A. Tiwari, K. Manoli, B. Holzer, N. Ditaranto, R.A. Picca, N. Cioffi, C. Di Franco, G. Scamarcio, G. Palazzo, L. Torsi, Label-free and selective single-molecule bioelectronic sensing with a millimeter-wide self-assembled monolayer of anti-immunoglobulins, Chem. Mater. 31 (2019) 6476–6483, https://doi.org/10.1021/acs.chemmater.8b04414.
[29] S.K. Sailapu, E. Macchia, I. Merino-Jimenez, J.P. Esquivel, L. Sarcina, G. Scamarcio, S.D. Minteer, L. Torsi, N. Sabaté, Standalone operation of an EGOFET for ultra-sensitive detection of HIV, Biosens. Bioelectron. 156 (2020) 1–7, https://doi.org/10.1016/j.bios.2020.112103.
[30] B. Holzer, K. Manoli, N. Ditaranto, E. Macchia, A. Tiwari, C. Di Franco, G. Scamarcio, G. Palazzo, L. Torsi, Characterization of covalently bound anti-human immunoglobulins on self-assembled monolayer modified gold electrodes, Adv. Biosyst. 1 (2017), https://doi.org/10.1002/adbi.201700055.
[31] T.J. Lenk, V.M. Hallmark, C.L. Hoffmann, J.F. Rabolt, D.G. Castner, C. Erdelen, H. Ringsdorf, Structural investigation of molecular organization in self-assembled monolayers of a semifluorinated amidethiol, Langmuir 10 (1994) 4610–4617, https://doi.org/10.1021/la00024a037.
[32] R.S. Clegg, J.E. Hutchison, Hydrogen-bonding, self-assembled monolayers: Ordered molecular films for study of through-peptide electron transfer, Langmuir 12 (1996), https://doi.org/10.1021/la960825f.
[33] P.A. Lewis, R.K. Smith, K.F. Kelly, L.A. Bumm, S.M. Reed, R.S. Clegg, J. D. Gunderson, J.E. Hutchison, P.S. Weiss, The role of buried hydrogen bonds in self-assembled mixed composition thiols on Au{111}, J. Phys. Chem. B. 105 (2001) 10630–10636, https://doi.org/10.1021/jp010854l.
[34] R.S. Clegg, J.E. Hutchison, Control of monolayer assembly structure by hydrogen bonding rather than by adsorbate-substrate templating, J. Am. Chem. Soc. 121 (1999) 5319–5327, https://doi.org/10.1021/ja9901011.
[35] R.S. Clegg, S.M. Reed, R.K. Smith, B.L. Barron, J.A. Rear, J.E. Hutchison, Interplay of lateral and tiered interactions in stratified self-organized molecular assemblies, Langmuir 15 (1999) 8876–8883, https://doi.org/10.1021/la9910529.
[36] S.-W. Tam-Chang, H.A. Biebuyck, G.M. Whitesides, N. Jeon, R.G. Nuzzo, Self-assembled monolayers on gold generated from alkanethiols with the structure RNHCOCH2SH, Langmuir 11 (1996) 4371–4382.
[37] R.G. Greenler, Infraredc study of adsorbed molecules on metal surfaces by reflection tehniques, J. Chem. Phys. 44 (1966) 310–315, https://doi.org/10.1063/1.1726462.

[38] R.G. Greenler, D.R. Snider, D. Witt, R.S. Sorbello, The metal-surface selection rule for infrared spectra of molecules adsorbed on small metal particles, Surf. Sci. 118 (1982) 415–428, https://doi.org/10.1016/0039-6028(82)90197-2.
[39] Z. Kuodis, I. Matulaitienė, M. Špandyreva, L. Labanauskas, S. Stončius, O. Eicher-Lorka, R. Sadzevičienė, G. Niaura, Reflection Absorption Infrared Spectroscopy Characterization of SAM Formation from 8-Mercapto-N-(phenethyl)octanamide Thiols with Phe Ring and Amide Groups, Mol. 25 (2020), https://doi.org/10.3390/molecules25235633.
[40] D. and Allara, J. Stapleton, Surface science techniques, 2013. https://doi.org/10.1007/978-3-642-34243-1.
[41] S.A. Swanson, R. McClain, K.S. Lovejoy, N.B. Alamdari, J.S. Hamilton, J.C. Scott, Self-assembled diisocyanide monolayer films on gold and palladium, Langmuir 21 (2005) 5034–5039, https://doi.org/10.1021/la047284b.
[42] S. Prati, M. Milosevic, G. Sciutto, I. Bonacini, S.G. Kazarian, R. Mazzeo, Analyses of trace amounts of dyes with a new enhanced sensitivity FTIR spectroscopic technique: MU-ATR (metal underlayer ATR spectroscopy), Anal. Chim. Acta. 941 (2016) 67–79, https://doi.org/10.1016/j.aca.2016.09.005.
[43] M. Milosevic, V. Milosevic, S.L. Berets, Grazing Angle Attenuated Total Reflection Spectroscopy: Fields at the Interface and Source of the Enhancement, Appl. Spectrosc. 61 (2007) 530–536. http://as.osa.org/abstract.cfm?URI=as-61-5-530.
[44] M.E. Mulcahy, S.L. Berets, M. Milosevic, J. Michl, Enhanced sensitivity in single-reflection spectroscopy of organic monolayers on metal substrates (Pseudo-ATR), J. Phys. Chem. B. 108 (2004) 1519–1521, https://doi.org/10.1021/jp036035d.
[45] S. Chah, J. Yi, C.M. Pettit, D. Roy, J.H. Fendler, Ionization and reprotonation of self-assembled mercaptopropionic acid monolayers investigated by surface plasmon resonance measurements, Langmuir 18 (2002) 314–318, https://doi.org/10.1021/la011226y.
[46] M. Milosevic, Internal reflection and ATR spectroscopy, 2012. https://doi.org/10.1081/ASR-200030195.
[47] E.D. Palik, Handbook of optical constants of solids, Handb. Opt. Constants Solids. 1 (2012) 1–804, https://doi.org/10.1016/C2009-0-20920-2.
[48] M.D. Porter, T.B. Bright, D.L. Allara, C.E. Chidsey, Spontaneously Organized Molecular Assemblies. 4. Structural Characterization of n-Alkyl Thiol Monolayers on Gold by Optical Ellipsometry, Infrared Spectroscopy, and Electrochemistry, J. Am. Chem. Soc. 109 (1987) 3559–3568, https://doi.org/10.1021/ja00246a011.
[49] R.G. Sinclair, A.F. McKay, R.N. Jones, The infrared absorption spectra of saturated fatty acids and esters, J. Am. Chem. Soc. 74 (1952) 2570–2575, https://doi.org/10.1021/ja01130a033.
[50] D. Sehgal, I.K. Vijay, A method for the high efficiency of water-soluble carbodiimide-mediated amidation, Anal. Biochem. 218 (1994) 87–91, https://doi.org/10.1006/abio.1994.1144.